ChemCatChem

The European Society Journal for Catalysis

Chemistry Europe

European Chemical Societies Publishing

Supported by GECATS GERMAN CATALYSIS SOCIETY

Accepted Article

Title: Selectivity Switch in the Aerobic 1,2-Propandiol Oxidation Catalyzed by Diamine-Stabilized Palladium Nanoparticles

Authors: Werner Oberhauser, Claudio Evangelisti, Laura Capozzoli, Gabriele Manca, Maria Pia Casaletto, and Francesco Vizza

To be cited as: *ChemCatChem* 10.1002/cctc.202100309

Link to VoR: https://doi.org/10.1002/cctc.202100309

WILEY-VCH

10.1002/cctc.202100309

Selectivity Switch in the Aerobic 1,2-Propandiol Oxidation Catalyzed by Diamine-Stabilized Palladium Nanoparticles

Werner Oberhauser,*[a] Claudio Evangelisti,[b] Laura Capozzoli,[a] Gabriele Manca,[a] Maria Pia Casaletto,[c] and Francesco Vizza[a]

[a] Dr. W. Oberhauser, Dr. L. Capozzoli, Dr. G. Manca, Dr. F. Vizza

Istituto di Chimica dei Composti Organometallici (CNR-ICCOM), Via Madonna del Piano 10, 50019 Sesto Fiorentino (Italy) E-mail: werner.oberhauser@iccom.cnr.it

[b] Dr. C. Evangelisti

Istituto di Chimica dei Composti Organometallici (CNR-ICCOM) U.O.S. di Pisa, Via G. Moruzzi 1, 56124 Pisa (Italy)

[c] Dr. M. P. Casaletto

Istituto per lo Studio dei Materiali NanoStrutturati (CNR-ISMN), Via Ugo La Malfa 153, 90146 Palermo (Italy)

Palladium nanoparticles stabilized by a sterically demanding secondary diamine ligand have been synthesized by hydrogen reduction of a palladium acetate complex bearing the corresponding diimine ligand. The obtained nanoparticles were used to catalyze the aerobic oxidation of 1,2-propandiol in *n*-hexane, and after their heterogenization onto a high surface area carbon, in water. In *n*-hexane (2,4-dimethyl-1,3-dioxolan-2-yl) methanol has been obtained as major product, whereas in water acetic acid with a selectivity of > 85% has been achieved. The selectivity switch observed was a clear induced by water. The robustness of diamine-stabilized palladium nanoparticles under real aerobic oxidation conditions has been proved by recycling experiments, TEM measurements of the recovered catalysts and by comparison of its performance with that of palladium nanoparticles generated by the metal vapor synthesis technique and supported onto the same carbon in the absence of the stabilizing diamine ligand.

Introduction

1,2-Propandiol (1,2-PD) is generally obtained by catalytic hydrogenolysis reactions of glycerol [1-5] and its further selective conversion under aerobic oxidation conditions to give either selectively hydroxyacetone or acetic acid is challenging. Indeed, aerobic metal nanoparticle (NP)-catalyzed 1,2-PD oxidation reactions conducted in neutral water results in a mixture of products comprising hydroxyacetone, lactic acid, pyruvic acid and formic acid. Catalytic reactions carried out with Pd-based catalysts in the presence of basic water solutions led to lactic acid as the main product, due to a base mediated intramolecular Cannizzaro reaction of pyruvaldehyde.[6-8] Basic supports (*e.g.* hydroxylapatite and $Mg(OH)_2$ showed to be important for efficient dehydrogenation reactions during the 1,2-PD conversion.[9,10] The highest acetic acid

selectivity in the aerobic 1,2-PD oxidation was obtained with Ag NPs in the presence of base (*i.e.* 63% acetic acid selectivity at complete 1,2-PD conversion at 120 °C)[11] and with a bimetallic Au-Pt catalyst supported onto carbon using neutral water solutions of 1,2-PD (*i.e.* 66% acetic acid selectivity at 82% 1,2-PD conversion at 115 °C).[12] The latter catalytic system gave also the highest selectivity for hydroxyacetone from 1,2-PD (*i.e.* 60% hydroxyacetone selectivity at 33% 1,2-PD conversion at 40 °C in the absence of base).

Hydroxacetone is an important platform molecule for the synthesis of renewable diesel[13] and the synthesis of higher oxygenates.[14] Its synthesis from glycerol occurs under harsh reaction conditions (*i.e.* vapor-phase dehydration at temperatures > 250 °C).[15-17] Also acetic acid, an important bulk molecule and mainly used for the synthesis of the vinylacetate monomer,[18] is produced in a more than 10 million tons scale by the Ir-based methanol carbonylation reaction (Cativa process).[19]

We herein report the synthesis of Pd NPs (**1**) obtained upon hydrogenation of an organometallic Pd(II) precursor.[20] **1** was efficiently stabilized by exerting the steric effect[21] of a secondary diamine ligand bearing *n*-hexadecyl groups at both nitrogen donor atoms. Amines featured by long aliphatic chains have been efficiently used in Pd-based hydrogenation,[22] Suzuki Miyaura coupling[23,24] and aerobic alcohol oxidation reactions.[25] **1** has been used to catalyze the aerobic oxidation of 1,2-PD in *n*-hexane and supported onto an high surface area carbon in neutral water.

Pd NPs are known to be a sensitizing agent causing allergic contact dermatitis.[26] Hence the application of a low amount of Pd-based catalyst combined with its recyclability is mandatory for a sustainable catalytic process.[27,28]

Results and Discussion

Synthesis and characterization of diamine-stabilized Pd NPs

The diimine ligand **L** (Scheme 1) reacted with a CH_2Cl_2 solution of $Pd(OAc)_2$ (OAc = acetate) at 35 °C in the presence of hydrogen (20 bar) for 18 h, giving a black suspension, which was concentrated to dryness. The dark brown residue was successively suspended in *n*-pentane and then filtered. The *n*-pentane insoluble fraction proved to be the ammonium salt of **H_4L** (Figure S5). The black *n*-pentane-soluble fraction was first extracted with water to remove the formed acetic acid (*i.e.* HPLC analysis of the water solution confirmed the presence of acetic acid) and then concentrated to dryness giving a black solid (**1**) (Scheme 1).

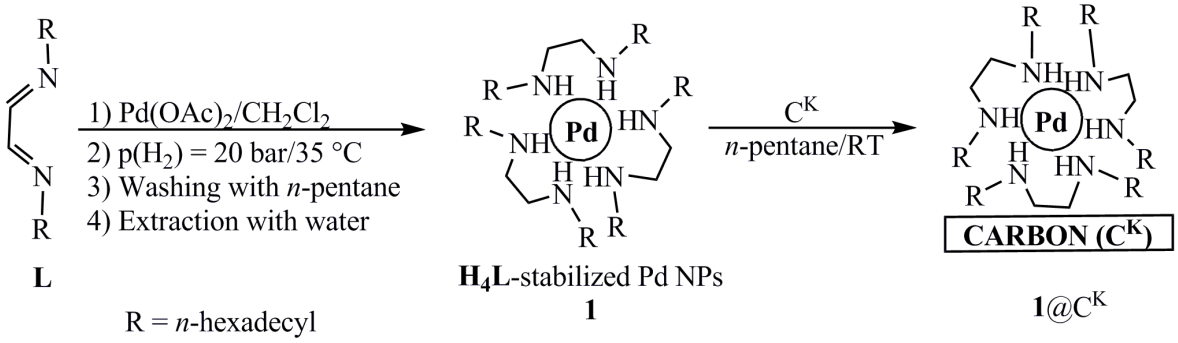

Scheme 1. Synthesis of **1** and **1**@C^K.

A STEM micrograph acquired for **1** (Figure 1) confirmed the presence of spherical, well-dispersed Pd NPs characterized by an average diameter of 3.6 ± 0.64 nm.

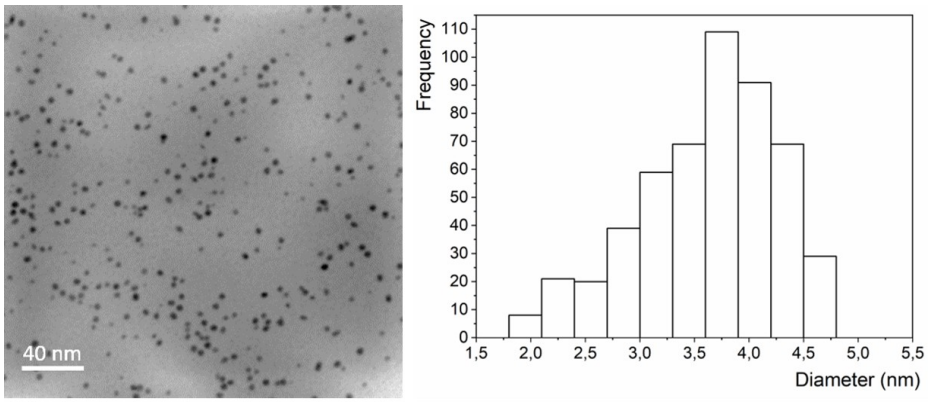

Figure 1. STEM micrograph and histogram for as-synthesized **1** (d_m= 3.6 ± 0.64 nm, N = 514).

The corresponding powder X-ray diffraction (PXRD) spectrum (Figure S6) showed Bragg reflexes, typical for fcc Pd, which were broad due to the small NPs' size. In addition, a Bragg reflex at 21.6 ° (2Θ) has been assigned to the crystalline fraction of the capping ligand. ICP-OES analysis of **1** exhibited a Pd content of 23.6 wt%.

The XPS curve-fitting of the Pd 3d spectrum acquired for **1** (Figure 2a) showed the presence of two distinct double peak components (Pd $3d_{5/2}$ and Pd $3d_{3/2}$ spin orbit splitted). In peak 1 Pd $3d_{5/2}$ located at BE = 335.3 eV and in peak 2 Pd $3d_{5/2}$ at BE = 337.9 eV can be assigned to Pd(0) and Pd(II) surface atoms in 48.1 and 51.9 peak area %, respectively (Table S1).[29] The N 1s photoelectron signal of **1** (Figure 2b), exhibited a slightly asymmetric peak, which revealed the presence of two components at BE = 399.7 eV (75.6 peak area %) and at BE = 400.7 eV (24.4 peak area %). A comparison of the N 1s spectra for **H_4L** and **1** (Figure 2b) clearly showed a shift of 0.7 eV of the main contribution (BE = 399.0 eV) to higher BE in case of **1** (BE = 399.7 eV). This shift of BE was attributed to the interaction of the amine functionality of **H_4L** with the Pd NPs' surface atoms.[30] The second component of the N 1s spectrum of **1** at BE = 400.7 eV was

assigned to a fraction of NH-groups undergoing hydrogen bond interactions with Pd-hydroxide species, the presence of which was also confirmed by the O 1s peak at BE = 532.0 eV (Figure S7).[31] The N to Pd atom ratio in **1** was shown to be 3 (Table S2).

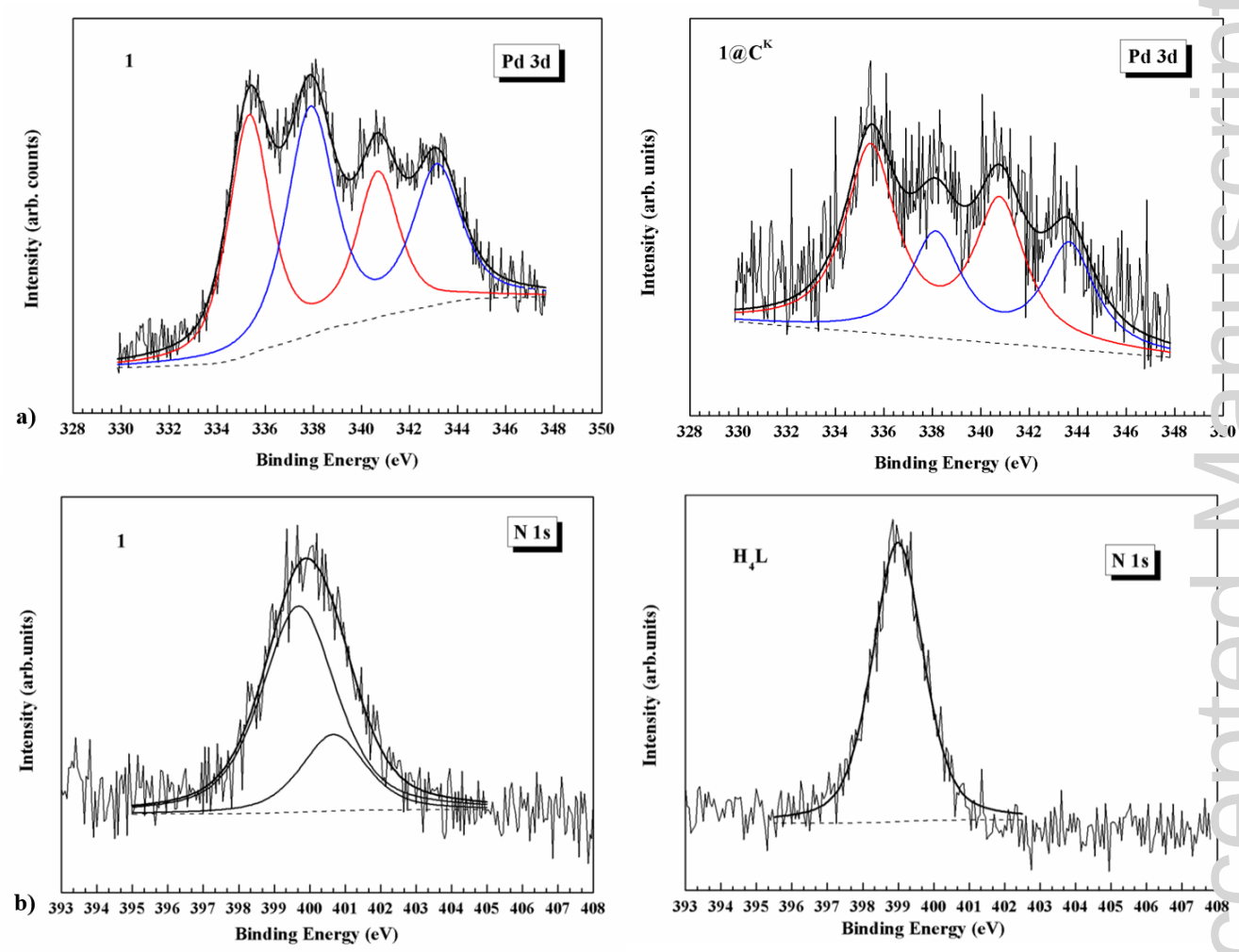

Figure 2. XPS curve-fitting of Pd 3d and N 1s spectra in the investigated samples, a) and b) respectively. In the Pd 3d region the red line refers to the Pd $3d_{5/2}$ and Pd $3d_{3/2}$ spin-orbit components of peak 1 and the blue line to those of peak 2.

The ^{1}H NMR spectrum acquired for **1** in C_6D_6 (Figure S8) clearly revealed a notable broadening of the NMR signals assigned to the nitrogen atoms-bridging methylene and the α-methylene groups of the C_{16}-alkyl chain at 2.31 and 2.68 ppm, respectively, due to their interaction with the surface NPs' Pd atoms.[32,33] Accordingly, the IR spectrum of **1**, acquired as KBr pellet, showed the absence of the N-H and C-N stretching bands, typically found for **H_4L** (KBr pellet) at 3238 cm^{-1} and 1130 cm^{-1}, respectively (Figure S9).

A parallel synthesis of **1**, following the same synthesis protocol as described in Scheme 1, but using **H_4L** to coordinate $Pd(OAc)_2$ instead of **L** brought about the formation of Pd NPs characterized by a huge size distribution (d_m = 3.0 ± 1.3 nm) (Figure S10). This experimental result is strongly indicating that the hydrogenation of **L** to **H_4L** does not occur at an early stage of the synthesis of **1**. Indeed, DFT-based calculations conducted with the molecular model compound M^1 (Scheme 2, see more details in SI) showed that upon reaction with hydrogen in CH_2Cl_2, acetic acid is formed through a dissociative acetate-based hydrogen activation process and that a final dimer Pd(I)hydride species with a two η^1-N coordinating diimine ligands (M^6) was obtained. The transformation of M^1 into M^6 has been associated to a free energy gain of 15.4 kcal mol^{-1} and the rate determining step for the conversion of M^1 to M^6 was the de-coordination of one acetate anion from M^1 giving M^2 (*i.e.* free energy cost of 18.4 kcal mol^{-1}). Any attempt to find a low free energy reaction path for the hydrogenation of the model diimine ligand to the corresponding diamine failed at this molecular level.

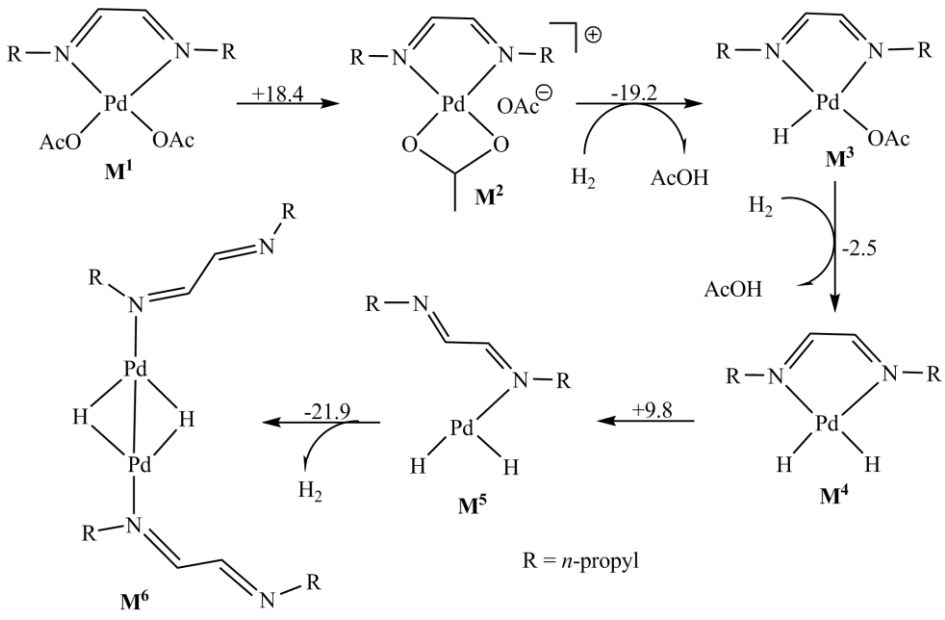

Scheme 2. DFT-based reaction path for the conversion of M^1 into M^6 in the presence of hydrogen and CH_2Cl_2. Free Gibbs energies are given in kcal mol^{-1}.

The importance of hexadecyl units in the stabilizing ligand of **1** for the NPs' dispersion was underscored by carrying out an analogous synthesis, as described in Scheme 1, using a diimine bearing *n*-butyl groups. As a result, Pd precipitated on the Teflon walls of the autoclave leading to a completely transparent CH_2Cl_2 solution.

In order to carry out catalytic aerobic1,2-PD oxidation reactions with **1** in neat water, **1** was supported onto Ketjenblack (C^K, high surface area carbon 1400 m^2/g)[34] by an impregnation method (Scheme 1) giving **1**@C^K with a Pd content of 1.28 wt% (ICP-OES analysis). A TEM micrograph of as-synthesized **1**@C^K (Figure 3) confirmed the presence of Pd NPs identical in average size to that of **1** (*i.e.* $d_m = 3.3 \pm 0.6$ nm (**1**@C^K) *vs* 3.6 ± 0.64 nm (**1**)).

10.1002/cctc.202100309

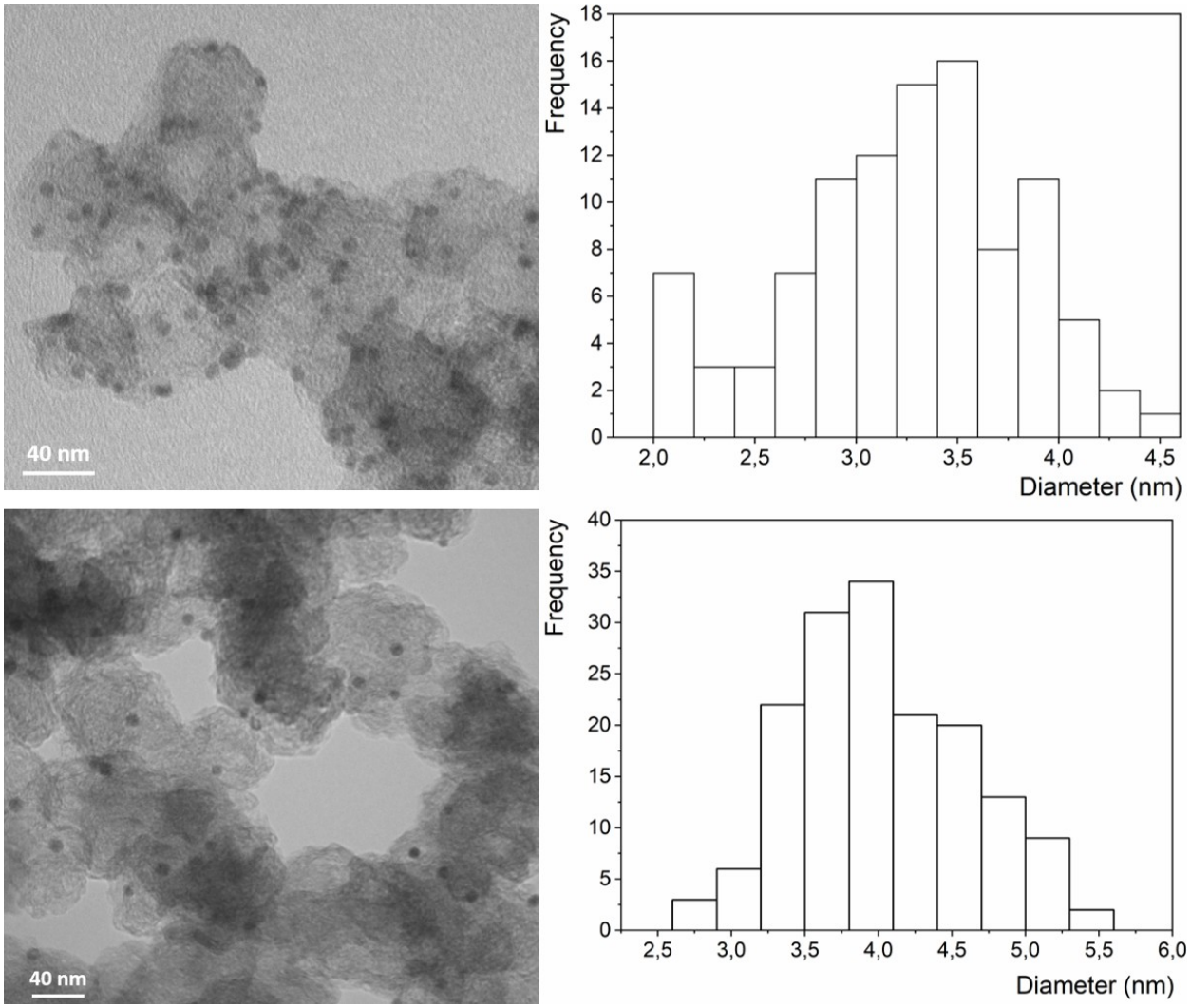

Figure 3. TEM micrographs and histograms for **1**@C^K: as-synthesized (d_m = 3.3 ± 0.6 nm, N = 101) (upper) and after catalysis (T = 140° C, t = 18h; d_m = 4.2 ± 1.34 nm, N = 168) (lower).

Also the Pd 3d XPS spectrum for **1**@C^K showed a Pd(0)/Pd(II) atom ratio of 61:39 (Figure 2a), which compared well with that of **1**. In order to validate the catalytic performance of **1**@C^K we introduced **Pd**@C^K as catalyst reference system. The latter catalyst was prepared by the metal vapor synthesis (MVS) technique and supported onto C^K in the absence of the stabilizing ligand **H_4L** (synthetic details are reported in the SI). The Pd loading was of 1.5 wt% and the spherical

NPs showed an average size of 2.5 ± 0.5 nm (Figure S11). For related NPs, synthesized by the same technique, a Pd(II)/Pd(0) ratio of 31.6/68.4 on the NPs' surface has been found.[35]

1-catalyzed aerobic 1,2-PD oxidation reactions in *n*-hexane

1-catalyzed aerobic oxidation reactions of 1,2-PD were conducted under biphasic reaction conditions (*i.e.* *n*-hexane solution of **1** and 1,2-PD, are not miscible at room temper) using air (20.0 bar) as final oxidant. The reaction products obtained under the latter catalytic condition are shown in Scheme 3 and the percentage of each product is compiled in Table 1 (entries 1-6).

In order to intercept all products formed during catalysis, methanol was added to the reaction mixture in order to separate the *n*-hexane phase, which confined the catalyst, from the reaction educts and products formed. The slightly yellow methanol solution has been analyzed by GC (*i.e.* using 1-hexanol as standard, Figure S12) and GC-MS. The carbon balance was found to be >95%. Regardless of the reaction temperature, (2,4-dimethyl-1,3-dioxolan-2-yl) methanol (**3**, Scheme 3) was found to be the major product (Table 1). Reaction temperatures lower than 110 °C let to a low substrate conversion (9.2 %), whereas upon its increase to 120 °C combined with a reaction time of 18h, the1,2-PD conversion increased to 85.7% (Table 1, entry 4). Under the latter experimental condition the side products (**4**, **5** and **6**, Scheme 3) were obtained with a selectivity of 3.6%, while **2** and **3** were present with 26.4 and 70.0 % selectivity, respectively. By carrying out a catalytic reaction in the presence of a small amount of water (100.0 μL), the 1,2-PD conversion dropped to 20.0% (*i.e* due to a drop in the mass transfer in the interphase), whereas the selectivity of **2** reached 58.0% at the expense of the ketal (*i.e*. hydrolysis of the ketal). In addition, under the latter reaction condition 8.0% of side products (7, 8, 9+10, Scheme 3) were found, with **8** being the major side product (6%).

The stability of **1** during catalytic reactions lasting 18h (110 °C) was proved by carrying out STEM analysis on recovered **1** from which emerged that the spherical Pd NPs' size increased only slightly in the course of the catalysis (d_m= 4.2 ± 1 nm (recovered **1**, Figure S13); d_m= 3.6 ± 0.64 nm (as-synthesized **1**, Figure 1)). A recycling experiment with **1** showed a slight drop of the 1,2-PD conversion to 78.0 %, while the product selectivity has found to be comparable to that obtained with as-synthesized **1** (Table 1, entry 6 *vs* entry 4). ICP-OES analysis of the separated methanol solution after catalysis showed a Pd content of 0.1 ppm, which corresponded to a Pd leaching of 0.05%.

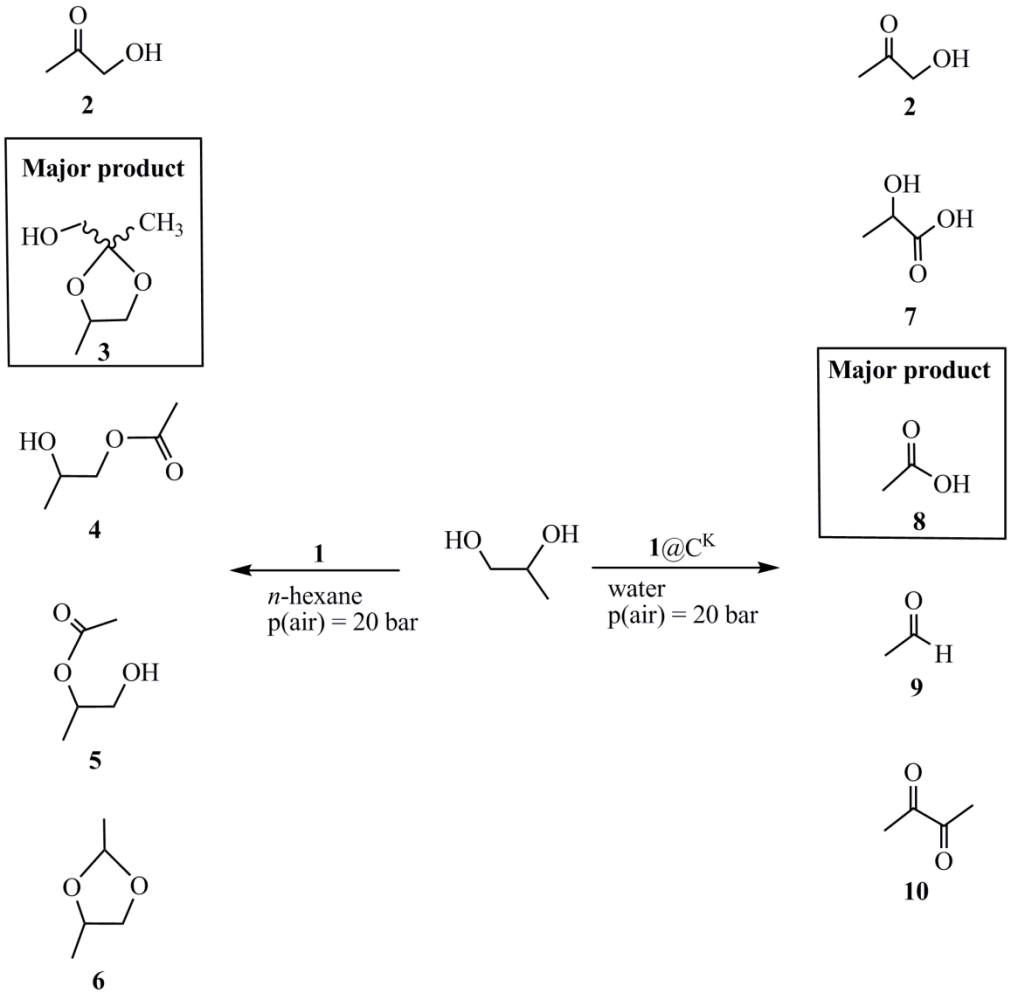

Scheme 3. Reaction products obtained in the **1**-and **1**@C^K-catalyzed aerobic 1,2-PD oxidation in *n*-hexane and water, respectively.

Table 1. Catalytic aerobic 1,2 PD oxidation with **1** in *n*-hexane and with **1**/ **Pd**@C^K in water.

Entry[a]	Cat.	Pd (mmol)	T [°C]/t [h]	Conv. 1,2 PD [%] [TOF(h^{-1})][b]	Selectivity [%][c]					
					2	**3**	**4+5+6**	**7**	**8**	**9+10**
1	**1**	0.051	100/5	9.2/[n.d.]	7.8	91.3	0.9			
2	**1**	0.051	110/5	18.2/[29]	12.5	86.1	1.4			
3	**1**	0.051	110/18	59.7/[26]	16.4	81.8	1.8			
4	**1**	0.051	120/18	85.7/[38]	26.4	70.0	3.6			
5[d]	**1**	0.051	120/18	20.0/[9]	58.0	34.0	-	1.0	6.0	1.0
6[e]	**1**	0.051	120/18	78.0/[n.d.]	28.2	68.0	3.8			
7	**1**@C^K	0.024	110/18	29.9[28]	53.2	-	-	18.0	26.6	2.2
8	**1**@C^K	0.024	120/18	45.0[42]	33.7	-	-	16.9	46.5	2.9
9	**1**@C^K	0.024	140/5	31.2[103]	41.0	-	-	4.0	51.7	3.3
10	**1**@C^K	0.024	140/18	89.1/[83]	7.0	-	-	5.0	85.0	3.0
11[e]	**1**@C^K	0.024	140/18	79/[n.d.]	13.1			2.0	83.0	1.9
12[f]	**1**@C^K	0.024	140/24	85.0/[118]	5.0			7.0	83.0	5.0
13	**Pd**@C^K	0.028	140/18	67.9/[43]	18.9			3.0	76.1	2.0
14[e]	**Pd**@C^K	0.028	140/18	41.0/[n.d.]	45.0			1.8	52.0	1.2

[a] Catalytic condition: 1,2-PD (13.70 mmol), solvent (50.0 mL), p(air) = 20.0 bar. [b] Surface atom-related TOF (h^{-1}). [c] Selectivity (%) defined as: 100 × [$mmol_{(Product)}$] × [Σ ($mmol_{(Products)}$]$^{-1}$. [d] Addition of water (100.0 µL). [e] 1st recycling. [f] 1,2-PD (27.40 mmol).

1@C^K-catalyzed aerobic 1,2-PD oxidation reactions in water

In order to carry out aerobic 1,2-PD oxidation reactions in water obtaining rational conversions, **1**@C^K was used instead of **1** as catalyst. **1**@C^K-mediated aerobic 1,2 PD oxidation reactions were carried out with neutral water solutions of 1,2-PD (0.274M and 0.548M) in the presence of air (20 bar) and in the temperature range between 110 and 140 °C (Table 1, entries 7-14). All catalytic solutions have been analyzed by HPLC (Figure S14), ^{1}H (Figure S15) and $^{13}C\{^1H\}$ NMR spectroscopy (Figure S16) and the intercepted products are shown in Scheme 3 and the results of the catalytic reactions in terms of 1,2-PD conversion and product selectivities are compiled in Table 1. Gas-phase analysis conducted after catalysis on the head space of the autoclave revealed the presence of CO_2 along with excess of air (Figure S17). A carbon balance

for the catalytic reactions in water in the temperature range from 110 to 140 °C has been found to of 95 and 90%, respectively. A blank reaction with 1,2-PD in water at 140 °C, 18h without **1**@C^K, showed no appreciable 1,2-PD conversion , underscoring the neat of **1**@C^K for a rational substrate conversion. At low 1,2-PD-conversions (110 °C, entry 7), **2** was the main product, whereas upon increasing the reaction temperature to 140 °C combined with a reaction time of 18h, **8** was the main product reaching a selectivity of 85.0% at a 1,2-PD conversion of 89.1% (Table 1, entry 10). The selectivity for **7** decreased with increasing temperature and remained comparable in reactions conducted at 140 °C with different 1,2-PD conversions, whereas the selectivity for **8** increased at the expense of **2** (Table 1, entry 10 *vs* 9). This latter experimental fact is strongly indicating that **8** has been generated via decarboxylation of pyruvic acid, originating from oxidation of **2** and not from oxidation of **7**.[36] In fact, efficient conversions of **7** to pyruvic acid have been reported for Mo-V-Nb-based mixed oxide catalysts at reaction temperatures > 200 °C[37] or for Au-Pt NPs supported onto acidic zeolites (140 ° C, $p(O_2)$ = 3 bar.[38] Pyruvic acid has not been intercepted as reaction intermediate in the aerobic oxidation of 1,2-PD to **8** in neat water, indicating that the decarboxylation of pyruvic acid is a fast reaction. Compounds **9** and **10** (Scheme 3) have been obtained in low amounts (1-5%, Table 1). Their formation during the catalytic reactions hints to the presence of a small amount of surface Pd-acyl species, which can recombine to give **10** and react with surface hydride species (*i.e.* originating from alcohol dehydrogenation reaction) leading to **9**.

Pd@C^K showed under identical catalytic conditions (140 °C, 18h) to be significantly less efficient compared to **1**@C^K in terms of surface-related TOF and selectivity for **8** (Table 1, entry 13 *vs* entry 10). Recycling experiments conducted with **1**@C^K and **Pd**@C^K lasting 18h clearly exhibited a significantly higher activity and selectivity drop for **8** in case of **Pd**@C^K (Table 1,

entry 14 *vs* entry 13 and entry 11 *vs* entry 10). TEM micrographs acquired for recovered **1**/**Pd**@C^K (*i.e*. reactions lasting 18h) confirmed a notable increase of the NPs' size during catalysis in case of **Pd**@C^K (d_m = 5.8 ± 1.6 nm, recovered **Pd**@C^K (Figure S18) *vs* d_m = 2.5 ± 0.5 nm, as-synthesized **Pd**@C^K (Figure S11)), whereas **1**@C^K showed a less pronounced increase of the NPs' size (*i.e*. 4.2 ± 1.34 nm, recovered **1**@C^K *vs* 3.3 ± 0.6 nm, as-synthesized **1**@C^K (Figure 3). The same result has been obtained by comparing the PXRD spectra of recovered **1**/**Pd**@C^K (Figure 4, trace c *vs* trace e). The PXRD spectrum of recovered **Pd**@C^K showed the presence of Bragg reflexes Pd(111), Pd(002) and Pd(022) which are typical for fcc Pd, whereas the PXRD spectrum of recovered **1**@C^K, which has been acquired applying the same acquisition parameters showed only a slight hump for Pd(111), confirming a smaller NPs' size in case of recovered **1**@C^K.

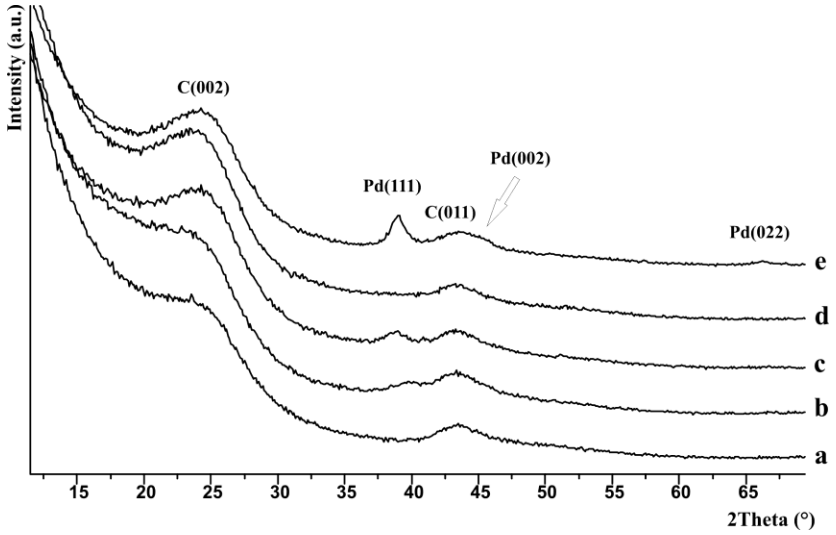

Figure 4. PXRD spectra acquired at room temperature for: C^K (a); **1**@C^K as-synthesized (b); **1**@C^K after catalysis (140 °C, 18h) (c); **Pd**@C^K as-synthesized (d) and **Pd**@C^K after catalysis (140 °C, 18h) (e).

ICP-OES analyses carried out on the water solutions, separated from the catalysts at 80 °C, after catalysis gave with both catalysts a Pd leaching of 0.05 ppm (*i.e.* 0.02% of the original Pd content), and by continuing the catalytic reaction without catalyst gave negligible 1,2-PD conversions. The different catalytic activity drop found for **1**/**Pd**@C^K can thus be associated to the different NPs' size increase observed for both catalysts.

The significantly higher robustness of **1**@C^K compared to **Pd**@C^K under aerobic 1,2-PD oxidation conditions let us to carry out an 1,2-PD oxidation with the former catalyst using a 1,2-PD water solution of 0.548M (*i.e.* molar ratio of 1,2-PD and surface Pd atoms of 3358). As a result, a surface atom related TOF value of 118 h^{-1} along with an acetic acid selectivity of 83.0% was obtained (Table 1, entry 12).

Catalytic cycle

1-catalyzed aerobic 1,2-PD oxidation reactions carried out in *n*-hexane comprises one dehydrogenation step to give hydroxyacetone (Scheme 4, reaction a), which leads upon a condensation reaction with excess 1,2-PD to the formation of (2,4-dimethyl-1,3-dioxolan-2-yl) methanol (Scheme 4, reaction f). The addition of water shifts the equilibrium of the condensation reaction in favor to free hydroxyacetone (*i.e.* a catalytic reaction carried out with **1** in neat *n*-hexane suppresses the hydrolysis of the acetal (Table 1)), which can further undergo an **1**-catalyzed dehydrogenation reaction (Scheme 4, reaction b) giving pyruvaldehyde. The latter compound is known to be a reactive intermediate which undergoes either a base-mediated Cannizzaro reaction[39] to lactic acid (*i.e.* **1**@C^K-catalyzed aerobic 1,2-PD (0.274 M) oxidation reaction carried out in the presence of an equimolar amount of NaOH at 140 °C for 18h, gave

lactic acid as main reaction product (lactic acid, 50.4% *vs* acetic acid, 41.1%), or reacts with water to give the corresponding pyruvacetal (Scheme 4, reaction c), which then dehydrogenate to give pyruvic acid (Scheme 4, reaction d). The three alcohol dehydrogenation reactions which converts 1,2-PD into PA (Scheme 4, reactions a, b and d) are catalyzed by surface Pd-OH species of **1**@C^K (XPS evidence), which are transformed into Pd-H (*i.e.* Pd-OH reacts with the alcohol to give the corresponding Pd-alcoholate and water and the former undergoes then a Pd-*β*-hydride elimination reaction giving Pd-H along with the release of the corresponding carbonyl or carboxyl species. Pd-H species on Pd NPs of an average size of 2.6 nm have been intercepted by a combination of X-ray absorption spectroscopy and X-ray diffraction.[40,41] The Pd-H species is retransformed into the Pd-OH species upon insertion of an oxygen molecule into the Pd-H species giving a Pd-hydroperoxide intermediate,[42] which reacts with water to give free hydrogen peroxide and Pd-OH. Hydrogen peroxide synthesis with Pd NPs in the presence of a H_2/O_2 mixture has been observed by operand spectroscopy.[43]

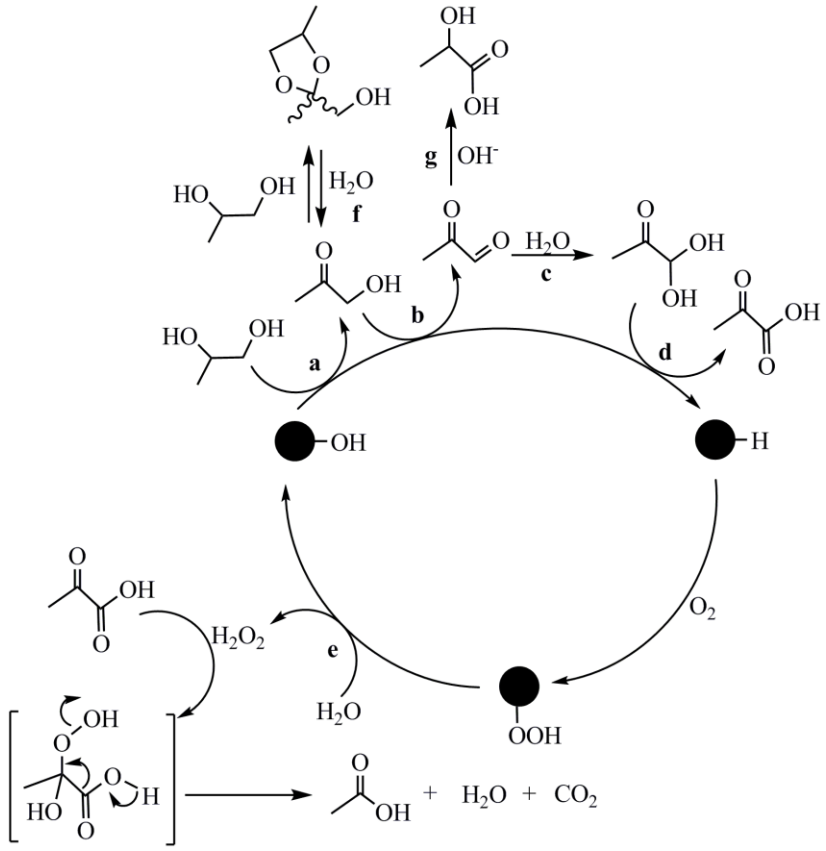

Scheme 4. Proposed catalytic cycle for the **1**-mediated aerobic 1,2-PD oxidation.

Hydrogen peroxide then nucleophlic attacks pyruvic acid leading to an oxidative decarboxylation of the latter and bringing about the formation of acetic acid, CO_2 and water. Indeed, the decarboxylation of pyruvic acid in water by hydrogen peroxide occurs already at 25 °C.[44] The need of **1**@C^K for a selective pyruvic acid decarboxylation reaction to occur has been proved by conducting parallel reactions with water solutions of pyruvic acid at 140 °C in the presence of 20 bar of air, with and without **1**@C^K. As a result, in the presence of the Pd-based catalyst pyruvic acid was quantitatively converted giving acetic acid with a selectivity of 99%, whereas in its

absence 70 % of pyruvic acid was converted to an 1:1 mixture of lactic acid and acetic acid. Hence in the absence of the catalyst pyruvic acid functions as hydride acceptor.

Conclusions

Pd NPs capped by secondary diamine ligand bearing C_{16}-alkyl chains at the nitrogen atoms (**1**) have been synthesized and successfully applied to catalyze the aerobic oxidation of 1,2-propandiol under biphasic catalytic conditions (*i.e*. using *n*-hexane solutions of **1**) and in water, after having supported **1** onto a carbon (**1**@C^K) featured by an high surface area. In the absence of water (2,4-dimethyl-1,3-dioxolan-2-yl) methanol (*i.e.* ketal formed between hydroxyacetone and 1,2-propandiol), whereas in the presence of water the same Pd-NPs converted 1,2-propandiol to acetic acid with a selectivity of 85% at 89% 1,2-propandiol conversion (*i.e*. 140 °C, 18h, p(air)= 20 bar), outperforming the best known catalytic system for the conversion of 1,2-propandiol to acetic acid, which uses a AuPt@C-based catalyst, 10 bar of oxygen at 115 °C for 24 h, leading to an acetic acid selectivity of 66% at a 1,2-propandiol conversion of 82%.[12] Water has an important role in the conversion of 1,2-propandiol to acetic acid under aerobic oxidation conditions, since it avoids the ketalization of hydroxyacetone by 1,2-propandiol. The pyruvic acid decarboxylation reaction to acetic acid is only selective in the presence of the palladium catalyst. The notable stabilizing effect of the diamine ligand on the Pd NPs is mainly steric in nature. On the other hand, the amine functionalities of the ligand might be involved in hydrogen bond interactions with water molecules close to the NPs' surface, fostering hence all reactions steps of the aerobic oxidation of 1,2-propandiol to acetic acid which need water to occur.

Experimental Section

Materials

Glyoxal (40wt% water solution), hexadecylamine, *iso*-propyl alcohol, $Pd(OAc)_2$, dichloromethane, methanol, *n*-hexane, *n*-pentane, C_6D_6, and $CDCl_3$ were purchased from Aldrich. Dichloromethane was distilled over CaH_2, methanol over Mg, while *n*-hexane and *n*-pentane were used as received. Ketjenblack (C^K) was purchased from Cabot Corp. USA.

Analytical methods

STEM (scanning transmission electron microscopy) images were acquired with a TESCAN GAIA 3 FIB/SEM apparatus using STEM detector operating at an accelerating voltage of 30 kV. TEM analyses were carried out on a TEM PHILIPS CM 12 instrument, equipped with an OLYPMPUS Megaview G2 camera, and using an accelerating voltage of 100 keV. Samples suitable for the analyses were prepared by depositing a drop of a *n*-pentane solution of **1** or water suspension of **1/Pd**@C^K on a holey film of a 300 mesh Cu grid, followed by evaporation of the solvent at room temperature. HRTEM micrographs were acquired with a ZEISS LIBRA 200 FE apparatus equipped with a 200 kV FEG source in column second generation omega filter. The mean particle diameter (d_m) was calculated by using the formula $d_m = \Sigma d_i n_i / \Sigma n_i$ with n_i corresponding to the number of particles with diameter d_i. The total number of particles (N) used for the histogram is reported in the caption of the corresponding figure.

Powder X-ray diffraction (PXRD) spectra were acquired at room temperature with a PANalytical X'PERT PRO powder diffractometer, using CuKα radiation (λ = 1.5418 Å) and a parabolic

MPD-mirror and a PIXcel RTMS detector. The spectra were recorded in the 2Θ range from 5.0 to 80.0 ° with a step size of 0.105 ° and a counting time of 428.9 s, using a Si zero background as sample holder.

X-ray photoelectron spectroscopy (XPS)-analyses of the samples was performed by using a XPS VG MicrotechESCA3000 Multilab spectrometer, equipped with a twin anode X-Ray source (Mg and Al) and a five channeltrons detection system. Photoemission spectra were acquired by using a standard non-monochromatized Al K_α (hν= 1486.6 eV) excitation source, an ultrahigh vacuum chamber (base pressure lower than 1×10^{-6} Pa) and a hemispherical analyser operating in CAE mode. The binding energy (BE) scale was calibrated with Au $4f_{7/2}$ core level at 83.9 eV. C 1s peak from the adventitious carbon (BE = 285.1 eV) was used for charge correction of all spectra. The accuracy of the energy measure is ± 0.1 eV. Photoemission data were collected and processed by VGX900 and XPSPEAK4.1 software, respectively. XPS data analysis was performed by a nonlinear least square curve-fitting procedure in order to extract chemical information from the spectra data (*i.e.* to separate the photoemission signal originating from distinct elemental or chemical states). A curve fitting model defined in terms of component peaks, as a properly weighted sum of Lorentzian and Gaussian component for the shape of Voight curves, and a Shirley background subtraction according to Sherwood[45] has been used. The fitting parameters that were allowed to vary for a component peak included the energy position, full width at half maximum (FWHM), the percentage of Lorentzian/Gaussian lineshape and area. The software used fitted the experimental data by adjusting all the parameters of the component peaks until a χ^2 minimum was obtained. The BE position of a component peak resulting from the curve fitting provided evidence for assignment to an elemental or chemical environment. Quantitative information concerning the concentration of the chemical states was

inferred by measuring the relative area of each component peak. C 1s, N 1s and O 1s spectra showed a single XPS peak, whereas Pd 3d showed a double peak with well separated Pd $3d_{5/2}$ and Pd $3d_{3/2}$ spin-orbit components (energy split of ~ 5.4 eV). Surface relative atomic concentrations were calculated by a standard quantification routine, including Wagner's energy dependence of attenuation length[46] and a standard set of VG Escalab sensitivity factors. The uncertainty on the atomic quantitative analysis is about ± 10%. Assignment of photoelectron signals and peak components was determined according to literature reference database.[47]

^{1}H and $^{13}C\{^{1}H\}$ NMR spectra were acquired in C_6D_6 at room temperature by using a Bruker Avance 400 MHz spectrometer. ^{1}H NMR spectra were acquired at 400.12 MHz and $^{13}C\{^{1}H\}$ NMR spectra at 100.0 MHz.

IR spectra were acquired as KBr pellets at room temperature in the wave number interval 4000-400 cm^{-1} using a Perkin Elmer instrument.

ICP-OES analysis were carried out with a ICP-Optical emission dual view Perkin Elmer OPTIMA 8000 apparatus.

HPLC analyses were carried out with a Shimadzu apparatus equipped with a RID 10A detector and an Aminex HPX-87H column (300 mm × 7.8 mm, BIO RAD) using H_2SO_4 (0.005 M) as eluent with a flow rate of 0.4 mL/min and an oven temperature of 35 °C.

GC analyses were carried out with a GC-2010 apparatus from Shimadzu, equipped with a FID and a capillary column of the type VF WAXms (30.0 m × 0.25 mm × 0.25 μm) from Agilent and He as carrier gas.

GC-MS analyses were carried out with a QP2010SE apparatus from Shimadzu, using the same capillary column as for GC analysis.

Syntheses of 1 and 1@C^{K}

Detailed protocols for the syntheses of **L**, **H$_4$L** and **Pd**@C^{K} are reported in the Supporting Information (SI).

L (343 mg, 0.680 mmol) (Scheme 1) and $Pd(OAc)_2$ (152.6 mg, 0.680 mmol) were added to a teflonated autoclave, which was sealed and evacuated. Afterwards dichloromethane (50.0 mL) was deareated and introduced into the autoclave by suction. The autoclave was then successively stirred at room temperature for one hour, followed by its pressurization with hydrogen (20 bar) and mechanical stirring at 35 °C for 18 hours. The autoclave was then successively cooled to 10 °C by means of a water-ice bath, the gas pressure released and the dark brown suspension transferred into a round bottom flask. The solvent was removed by vacuum and the brown residue suspended in *n*-pentane (50.0 mL), followed by filtration over celite. The obtained dark brown solution was extracted with water (3×10 mL) (*i.e.* to remove acetic acid, which was formed during the reaction), dried over Na_2SO_4, filtered and concentrated to dryness. In order to obtain the product as powder, the solid was dissolved in dichloromethane (10.0 ml) and then concentrate again to dryness, obtaining a dark brown solid. Yield: 110 mg. ICP-OES analysis of **1** showed a Pd content of 23.6 wt%. ^{1}H NMR (C_6D_6) and IR (KBr) spectra are shown in SI, Figure S8 and S9, respectively.

1@C^{K} was synthesized by suspending Ketjenblack (C^{K}) (1.0 g) in *n*-pentane (180.0 mL) followed by sonication for 5 min. at room temperature, addition of **1** (54.2 mg) dissolved in *n*-

pentane (30.0 mL), stirring for an hour under a nitrogen atmosphere and then evaporating the solvent by vacuum. The obtained black solid was continued drying at 50 ° C under vacuum. The Pd content of the isolated solid was analyzed by ICP-OES, giving a Pd content of 1.28 wt%.

Catalytic aerobic 1,2-PD oxidation reactions

Catalytic reactions in *n*-hexane

1 (23.22 mg, 0.051 mmol) was dissolved in *n*-hexane (50.0 mL) and transferred into a teflonated steel autoclave (320.0 mL). To the clear dark brown solution was added 1,2-PD (1.0 mL, 13.7 mmol) at room temperature. The autoclave was then successively sealed, heated to the desired reaction temperature, pressurized with air (20 bar) and magnetically stirred (1000 rpm). After the catalytic reaction, the autoclave was cooled to 10 °C by means of a water-ice bath, slowly vented and methanol (10.0 mL) added. The resulting suspension was stirred, the methanol phase separated from *n*-hexane solution and *n*-hexanol (standard, 200 μL) was added to the former solution. The methanol solution was analyzed by GC and GC-MS and each product was quantified by means of GC analysis using calibration curves. For the recycling experiment, the recovered *n*-hexane solution of **1** was reused.

Catalytic reactions in water

A teflonated autoclave (320.0 mL) was successively charged with **1**@C^K (200.0 mg), Pd (1.28 wt%, 0.024 mmol) or **Pd**@C^K (200.0 mg) Pd (1.5 wt%, 0.028 mmol) and a water solution (50.0 mL) of 1,2-PD (0.274M or 0.548M) sealed, heated to the desired reaction temperature,

pressurized with air (20 bar) and mechanically stirred (1000 rpm) for the desired reaction time. Afterwards, the autoclave was cooled to 10 °C and the gas slowly vented. A fraction of this venting gas was collected for gas analysis, which was carried out with a GC apparatus from Shimadzu, equipped with a TCD. Thereafter the autoclave was opened and the suspension filtered. The solution was analyzed by ^{1}H, $^{13}C\{^{1}H\}$NMR spectroscopy using an Evans tube which contained D_2O and by HPLC. For recycling experiments, the recovered **1**@C^K and **Pd**@C^K were washed with water (2 × 20 mL) and then dried in a vacuum oven at 50 °C, prior to their reuse in catalysis.

The surface atom related TOF values (h^{-1}), reported in Table 1 were calculated based on the following equation:

$$TOF = [mmol_{(converted\ 1,2\text{-}Pd)}] \times [mmol_{(Pd\ surface\ atoms)} \times h]^{-1}.$$

The amount of surface Pd-atoms in **1/Pd**@C^K has been determined by means of the corresponding TEM histograms.[48] As a result, **1**@C^K and **Pd**@C^K showed a Pd-surface atom fraction of 34 and 43%, respectively. 200 mg of **1**@C^K and **Pd**@C^K (amount of catalyst used, Table 1) contained 8.2 and 12.0 μmol of surface Pd atoms, respectively.

The mass balance of the reactions was calculated based on the following equation:

$$\text{Mass balance (\%)} = [mmol_{(liquid\ products)} + mmol_{(residual\ 1,2\text{-}PD)} + mmol_{CO2}] \times [mmol_{(1,2\text{-}PD\ initial)}]^{-1} \times 100$$

Oxidative decarboxylation of pyruvic acid in water

A teflonated autoclave (320.0 mL) was charged with a water solution (50.0 mL) of PA (13.8 mmol), sealed, heated to 140 °C and charging with air (20 bar). The autoclave was then stirred at the latter temperature for 18 h and was then successively cooled by means of an ice bath to 10 °C, the gas pressure released and the solution analyzed by HPLC. The same experimental procedure was applied for the reaction conducted in the presence of **1**@C^K (*i.e.* the same amount of **1**@C^K as used for 1,2-PD oxidation reactions (Table 1) has been used).

Acknowledgments

The authors thank the Italian National Research Council (CNR) microscopy facility "Ce.M.E.–Centro Microscopie Elettroniche Laura Bonzi" for providing the facilities for the Gaia 3 (Tescan s.r.o, Brno, Czech Republic) instrument acquired thanks to "Ente Cassa di Risparmio di Firenze" Grant Number n. 2013.0878, Regione Toscana POR FESR 2014-2020 and the project FELIX (Fotonica ed Elettronica Integrata per l' Industria), Grant Number 6455.

Conflict of interest

The authors declare no conflict of interest.

Keywords: heterogeneous catalysis, air, oxidation, 1,2-propandiol, palladium

[1] J. ten Dam, U. Hanefeld, *ChemSusChem* **2011**, *4*, 1017-1034.

[2] D. Roy, B. Subramaniam, R. V. Chaudhari, *Catal. Today* **2010**, *156*, 31-37.

[3] E. P. Maris, W. C. Ketchie, M. Murayama, R. J. Davis, *J. Catal*. **2007**, *251*, 281-294.

[4] A. Bienholz, H. Hofmann, P. Claus, *Appl. Catal. A* **2011**, *391*, 153-157.

[5] M. A. Dasari, P.-P. Kiatsimkul, W. R. Sutterlin, G. J. Suppes, *Appl. Catal. A* **2005**, *281*, 225-231.

[6] Y. Ryabenkova, Q. He, P. J. Miedziak, N. F. Dummer, S. H. Taylor, A. F. Carley, D. J. Morgan, N. Dimitratos, D. J. Willock, D. Bethell, D. W. Knight, D. Chadwick, C. J. Kiely, G. J. Hutchings, *Catal. Today* **2013**, *203*, 139-145.

[7] M. B. Griffin, A. A. Rodriguez, M. M. Montemore, J. R. Monnier, C. T. Williams, J. W. Medlin, *J. Catal*. **2013**, *307*, 111-120.

[8] N. Dimitratos, J. A. Lopez-Sanchez, S. Meenakshisundaram, J. M. Anthonykutty, G. Brett, A. F. Carley, S. H. Taylor, D. W. Knight, G. J. Hutchings, *Green Chem*. **2009**, *11*, 1209-1216.

[9] Y. Feng, H. Yin, D. Gao, A. Wang, L. Shen, M. Meng, *J. Catal.* **2014**, *316*, 67-77.

[10] Y. Feng, H. Yin, A. Wang, D. Gao, X. Zhu, L. Shen, M. Meng, *Appl. Catal. A* **2014**, *482*, 49-60.

[11] Y. Feng, H. Yin, A. Wang, W. Xue, *J. Catal.* **2015**, *326*, 26-37.

[12] Y. Ryabenkova, P. J. Miedziak, N. F. Dummer, S. H. Taylor, N. Dimitratos, D. J. Willock, D. Bethell, D. W. Knight, G. J. Hutchings, *Top. Catal*. **2012**, *55*, 1283-1288.

[13] G. Li, N. Li, S. Li, A. Wang, Y. Cong, X. Wang, T. Zhang, *Chem. Commun*. **2013**, *49*, 5727-5729.

[14] D. Enders, M. Voith, A. Lenzen, *Angew. Chem. Int. Ed*. **2005**, *44*, 1304-1325; *Angew. Chem*. **2005**, *117*, 1330-1351.

[15] D. C. Carvalho, L. G. Pinheiro, A. Campos, E. R. C. Millet, F. F. de Sousa, J. M. Filho, G. D. Saraiva, E. C. da Silva Filho, M. G. Fonseca, A. C. Oliveira, *Appl. Catal. A* **2014**, *471*, 39-49.

[16] S. Sato, D. Sakai, F. Sato, Y. Yamada, *Chem. Lett*. **2012**, *41*, 965-966.

[17] A. K. Kinage, P. P. Upare, P. Kasinathan, Y. K. Hwang, J.- S. Chang, *Catal. Commun*. **2010**, *11*, 620-623.

[18] D. Kumar, M. S. Chen, D. W. Goodman, *Catal. Today* **2007**, *123*, 77-85.

[19] G. J. Sunley, D. J. Watson, *Catal. Today* **2000**, *58*, 293-307.

[20] N. J. S. Costa, M. Gurrero, V. Colliére, E. Teixeira-Neto, R. Landers, K. Philippot, L. M. Rossi, *ACS Catal*. **2014**, *4*, 1735-1742.

[21] L. M. Rossi, J. L. Fiorio, M. A. S. Garcia, C. P. Ferraz, *Dalton Trans*. **2018**, *47*, 5889-5915.

[22] B. Wu, H. Huang, J. Yang, N. Zheng, G. Fu, *Angew. Chem. Int. Ed*. **2012**, *51*, 3440-3443; *Angew. Chem*. **2012**, *124*, 3496-3499.

[23] V. B. Saptal, M. V. Saptal, R. S. Mane, T. Sasaki, B. M. Bhanage, *ACS Omega* **2019**, *4*, 643-649.

[24] O. Verho, A. Nagendiran, E. V. Johnston, C. Tai, J.-E. Bäckvall, *ChemCatChem* **2013**, *5*, 612-618.

[25] S. Shimazu, T. Uehara, A. Asami, T. Hara, N. Ichikuni, *J. Mol. Catal. A* **2008**, *282*, 28-33.

[26] F. L. Filon, M. Crosera, M. Mauro, E. Baracchini, M. Bovenzi, T. Montini, P. Fornasiero, G. Adami, *Environmental Pollution* **2016**, *214*, 497-503.

[27] M. Monai, M. Melchionna, P. Fornasiero, *Adv. Catal*. **2018**, *63*, 1-73.

[28] V. Gombac, T. Montini, A. Falqui, D. Loche, M. Prato, A. Genovese, M. L. Mercuri, A. Serpe, P. Fornasiero, P. Deplano, *Green Chem*. **2016**, *18*, 2745-2752.

[29] R. Arrigo, M. E. Schuster, Z. Xie, Y. Yi, G. Wowsnick, L. L. Sun, K. E. Hermann, M. Friedrich, P. Kast, M. Hävecker, A. Knop-Gericke, R. Schlögl, *ACS Catal*. **2015**, *5*, 2740-2753.

[30] Q. Zhao, Y. Zhu, Z. Sun, Y. Li, G. Zhang, F. Zhang, X. Fan, *J. Mat. Chem. A* **2015**, *3*, 2609-2616.

[31] S. Kerber, J. J. Bruckner, K. Wozniak, S. Seal, S. Hardcastle, T. L. Barr, *J. Vac. Sci. Technol. A* **1996**, *14*, 1314-1320.

[32] L. E. Marbella, J. E. Millstone, *Chem. Mater.* **2015**, *27*, 2721-2739.

[33] G. Salassa, T. Bürgi, *Nanoscale Horizons* **2018**, *3*, 457-463.

[34] W. Oberhauser, C. Evangelisti, R. P. Jumde, R. Psaro, F. Vizza, M. Bevilacqua, J. Filippi, B. F. Machado, P. Serp, *J. Catal.* **2015**, *325*, 111-117.

[35] W. Oberhauser, C. Evangelisti, R. P. Jumde, G. Petrucci, M. Bartoli, M. Frediani, M. Mannini, L. Capozzoli, E. Passaglia, L. Rosi, *J. Catal*. **2015**, *330*, 187-196.

[36] L. Prati, M. Rossi, *J. Catal*. **1998**, *176*, 552-560.

[37] S. Lomate, B. Katryniok, F. Dumeignil, S. Paul, *Sustain. Chem. Process* **2015**, *3*, 5.

[38] R. K. Pazhavelikkakath Purushothaman, J. van Haveren, A. Mayoral, I. Melián-Cabrera, H. J. Heeres, *Top. Catal*. **2014**, *57*, 1445-1453.

[39] M. Marczewski, Y. Kavalchuk, U. Ulkowska, M. Gliński, O. Osawaru, *React. Kinet. Mech. Catal.* **2019**, *126*, 199-217.

[40] A. L. Bugaev, A. A. Guda, K. A. Lomachenko, V. V. Shapovalov, A. Lazzarini, J. G. Vitillo, L. A. Bugaev, E. Groppo, R. Pellegrini, A. V. Soldatov, J. A. van Bokhoven, C. Lamberti, *J. Phys. Chem. C* **2017**, *121*, 18202-18213.

[41] A. L. Bugaev, A. A. Guda, A. Lazzerini, K. A. Lomachenko, E. Groppo, R. Pellegrini, A. Piovano, H. Emerich, A. V. Soldatov, L. A. Bugaev, V. P. Dmitriev, J. A. van Bokhoven, C. Lamberti, *Catal. Today* **2017**, *283*, 119-126.

[42] B. V. Popp, S. S. Stahl, *J. Am. Chem. Soc.* **2007**, *129*, 4410-4422.

[43] M. Selinsek, B. J. Deschner, D. E. Doronkin, T. L. Sheppard, J.-D. Grunwaldt, R. Dittmeyer, *ACS Catal*. **2018**, *8*, 2546-2557.

[44] A. Lopalco, G. Dalwadi, S. Niu, R. L. Schowen, J. Douglas, V. J. Stella, *J. Pharm. Sci.* **2016**, *105*, 705-713.

[45] P. M. A. Sherwood, D. Briggs, M. P. Seah, (Eds.) Data analysis in X-ray photoelectron spectroscopy in practical surface analysis by Auger and X-ray photoelectron spectroscopy, Wiley, New York 1990 p. 1

[46] C. D. Wagner, L. E. Davis, W. M. Riggs, *Surf. Interface Anal*. **1980**, *2*, 53-55.

[47] NIST Standard Reference Database 20, Version 3.4

[48] A. Borodziński, M. Bonarowska, *Langmuir* **1997**, *13*, 5613-5620.

10.1002/cctc.202100309

Table of contents graphic

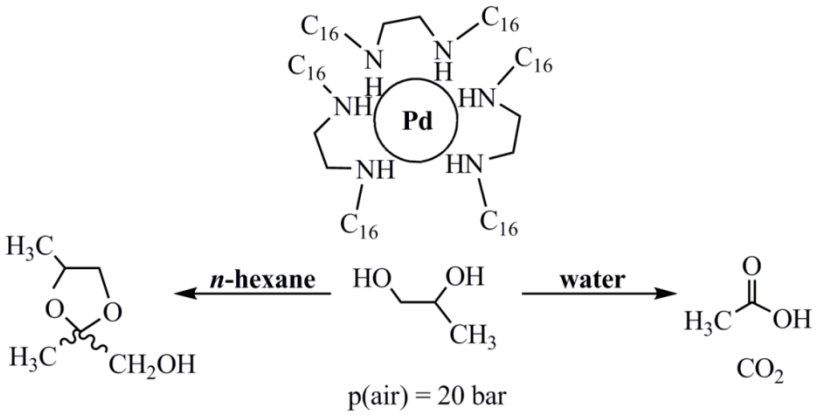

(2,4-dimethyl-1,3-dioxolan-2-yl) methanol *vs* acetic acid: Hexane solutions of the diamine-stabilized palladium nanoparticles efficiently catalyzed the aerobic oxidation of 1,2-propandiol, giving (2,4-dimethyl-1,3-dioxolan-2-yl) methanol as major compound, whereas the same nanoparticles oxidized in water 1,2-propandiol to acetic acid. The selectivity switch was triggered by water.